Acta Biomaterialia 7 (2011) 1140–1149

Contents lists available at ScienceDirect

Acta Biomaterialia

journal homepage: www.elsevier.com/locate/actabiomat

Mathematical modeling of degradation for bulk-erosive polymers: Applications in tissue engineering scaffolds and drug delivery systems

Yuhang Chen, Shiwei Zhou, Qing Li *

School of Aerospace, Mechanical and Mechatronic Engineering, University of Sydney, Sydney, NSW 2006, Australia

ARTICLE INFO

Article history:
Received 23 June 2010
Received in revised form 7 September 2010
Accepted 28 September 2010
Available online 16 October 2010

Keywords:
Biodegradation
Biodegradable polymers
Autocatalysis
Microparticle
Scaffold

ABSTRACT

The degradation of polymeric biomaterials, which are widely exploited in tissue engineering and drug delivery systems, has drawn significant attention in recent years. This paper aims to develop a mathematical model that combines stochastic hydrolysis and mass transport to simulate the polymeric degradation and erosion process. The hydrolysis reaction is modeled in a discrete fashion by a fundamental stochastic process and an additional autocatalytic effect induced by the local carboxylic acid concentration in terms of the continuous diffusion equation. Illustrative examples of microparticles and tissue scaffolds demonstrate the applicability of the model. It is found that diffusive transport plays a critical role in determining the degradation pathway, whilst autocatalysis makes the degradation size dependent. The modeling results show good agreement with experimental data in the literature, in which the hydrolysis rate, polymer architecture and matrix size actually work together to determine the characteristics of the degradation and erosion processes of bulk-erosive polymer devices. The proposed degradation model exhibits great potential for the design optimization of drug carriers and tissue scaffolds.

1. Introduction

Degradable biomaterials, such as polymers, have drawn significant attention recently for their extensive application in a range of new fields, e.g. scaffold tissue engineering and drug delivery systems [1–3]. In general, biodegradable polymers undergo a series of bioprocesses after being implanted in the human body which could dynamically affect the local biochemical and biophysical environment in a number of ways, including: (1) hydrolysis or other forms of chemical breakdown that produce oligomers and monomers in the polymeric matrix; (2) mass transport inside the polymer matrix and exchange of these products with the surroundings; (3) bioabsorption of the degraded biocompatible products. In this context, substantial experimental studies have been conducted to help better understand the mechanisms of biodegradation in such a complex process [4].

Although polymer degradation involves various complex chemical reactions, it is more often accompanied by multifaceted physical processes. Conceptually, degradation is defined as the molecular changes due to chain scission inside a polymer matrix, while erosion indicates the phenomenological and structural changes due to mass loss of degraded chains. Although detailed mechanisms have not yet been fully understood, extensive experimental studies have been conducted to explore the degradation and erosion pathways. Chain scission of the polymer matrix takes place when adjacent water molecules attack the chemical bonds, immediately after the surrounding solution starts to penetrate the matrix. As a result, both the speed of penetration and the hydrolysis rate can determine the degradation pattern. In essence, polymeric erosion has been categorized as following either 'bulk' or 'surface' pathways [5,6]. If the water penetration speed is considerably faster than the natural hydrolysis rate, e.g. as for polylactide (PLA) and polyglycolide (PGA) materials, degradation should take place over the entire polymer matrix, leading to a uniform mode of erosion, termed the 'bulk' pathway. On the other hand, if the diffusion of water molecules is relatively slow, hydrolysis will mostly happen in the form of surface erosion. Typically, such erosion is largely restricted to the exterior, while the interior remains almost unchanged, leading to an erosive front at the matrix surface which could proceed at a nearly constant velocity, termed 'surface' pathway. Nevertheless, these two extreme cases can happen concurrently for some materials with sophisticated configurations, which could greatly affect drug release and tissue regeneration within biodegradable synthetics. For this reason, the modeling of biodegradable devices is a crucial step towards regulating and controlling the degradation process.

For some commonly used biodegradable polymers, e.g. PLA and PGA, the hydrolytic products can result in a high concentration of carboxyl end groups that are specific catalysts of the hydrolysis reaction. If these products cannot be removed from the matrix within a certain period of time, acid catalyst in the polymer bulk

* Corresponding author. Tel.: +61 2 9351 8607; fax: +61 2 9351 7060.
E-mail address: Qing.Li@Sydney.edu.au (Q. Li).

1742-7061/$ - see front matter © 2010 Acta Materialia Inc. Published by Elsevier Ltd. All rights reserved.
doi:10.1016/j.actbio.2010.09.038

Nomenclature

x	status variable for degradation cells. 'Hydrolysable' ($x_H = 1$), 'hydrolyzed' ($x_h = 0.001$) and 'void' ($x_v = 0$)	C_m	concentration profile of released monomers
M_a	average molecular weight	n	number of nodes for a degradation element
λ	experimental degradation rate constant	D_m^0	diffusivity of released monomers before degradation
λ_0	autocatalysis-free degradation rate constant	D_m	diffusivity of released monomers during degradation
p	hydrolysis probability density function	R_m	material constant for the diffusivity change after hydrolysis
α	initial architectural porosity	β	parameter that regulates the autocatalysis effect for matching the modeling results to known experimental data
t_{add}	hysteretic degradation time for a polymer matrix with initial architectural porosity α		
V	volume fraction of polymer matrix during degradation		

will greatly accelerate the local hydrolytic process and consequently produce a hull-like distribution of molecular weight. Thus, autocatalysis plays an important role in the degradation rate and erosion pathway, thereby making the design of synthetic biodegradable matrices size dependent [7–12]. If the thickness of the polymer wall (i.e. the diffusion path) is sufficiently small and the hydrolysis products diffuse quickly, the acid catalysts can be rapidly removed by mass diffusion. Thus autocatalysis would be largely suppressed [13]. It should be noted that, due to the mechanism of erosion, the autocatalytic effect becomes more significant in bulk-erosive polymer devices [6]. Agrawal et al. [14] examined the effects of fluid flow on the degradation characteristics of biodegradable scaffolds *in vitro* and found that the degradation rate can be greatly decreased by fluid flow, suggesting that the autocatalytic effect plays an important role in altering the scaffold degradation process. Nevertheless, the impact of autocatalysis on polymer degradation and erosion lacks quantitative characterization to date, often leading to an imprecise prediction to the performance of biodegradable devices.

In terms of the better design of biodegradable devices, mathematical modeling has proved effective by extending the knowledge obtained from degradation experiments [15]. The literature shows that there are two main categories of mathematical models available to date, namely discrete and continuous schemes, which allow the simulation of polymeric degradation and erosion in different scenarios. On the one hand, discrete element-based models, as in Zygourakis [16] and Zygourakis and Markenscoff [17], are widely accepted as taking into account both the degradation and erosion processes. In this respect, Gopferich and co-workers [18–20] considered hydrolysis to be a stochastic process using a percolation-based erosion model, where both the 'bulk' and 'surface' pathways were phenomenologically simulated. Later, Bertrand et al. [21] modeled drug release from bioerodible microspheres using a cellular automaton method in which the polymer matrix was represented by elements in different states. Barat et al. [22] further proposed a cellular automata (CA) agent-based Monto Carlo (MC) model to simulate protein release from PLGA nano- and micro-particles. All these discrete models exploited the individual cells or elements to deal with complicated degradation and erosion processes.

Continuous models governed by partial differential equations have also been widely adopted to model the degradation process [23]. In this respect, Thombre and Himmelstein [24] proposed a diffusion–reaction model to describe controlled drug release that took into account the unsteady-state mass equilibrium for all components within bioerodible polymers. More recently, Wang et al. [25] developed a phenomenological model to simulate the degradation process based on the diffusion–reaction equation, and further investigated the interplay between crystallization and degradation [26]. In addition, Rothstein et al. [27] derived a mathematical model for predicting drug release from polymer matrices by both the surface and bulk pathways, in which the transition from surface to bulk erosion characteristics was explored. Soares and Zunino [28] also proposed a mixed model that can quantify the water-dependent degradation and erosion of drug delivery systems. More details of the mathematical methods used to characterize the degradation and erosion of biodegradable polymers can be found in recent review articles [15,23].

The development of scaffold tissue engineering and advanced drug delivery systems often necessitates consideration of other issues, such as the oxygen concentration and mechanical stimulation, rather than only the degradation itself. Although the continuous model involving a diffusion equilibrium and hydrolysis products appears straightforward in characterizing complicated degradation scenarios, the finite element-based design of biomedical devices shows certain benefits, along with the rapidly developing technology of solid free-form fabrication (SFF) [1,29,30], through which physical, mechanical and fluidic analyses can be readily conducted for sophisticated scaffold structures and other synthetic porous constructs. To facilitate such multi-fold analyses, it appears essential to integrate the continuous mass diffusion process into the discrete model.

In this paper we propose a hybrid mathematical model that combines stochastic hydrolysis and diffusion-governed autocatalysis to simulate polymer degradation and erosion for bulk-erosive biodegradable devices. Specifically, a reduced degradation rate constant that eliminates size-dependent effect of hydrolysis and a regulating parameter that takes into account autocatalysis are both considered. The examples, including drug delivery microparticles and tissue scaffolds, illustrate the degradation and erosion processes for polymeric devices of different sizes and with different architectures, thus addressing the size-effect and the need for design of biodegradable devices.

2. Methods

2.1. Basic assumptions

Consider a biodegradable polymer with an arbitrary configuration in a regular design domain that is uniformly discretized into a finite number of degradation elements (cells). Variable x is assigned for each element, indicating three different states of degradation, "hydrolysable" ($x_H = 1$), "hydrolyzed" ($x_h = 0.001$) and "void" ($x_v = 0$), respectively. For the sake of simplicity, the size distribution of polymer chains and initial density are assumed to be uniform throughout the polymer matrix. Therefore, it is assumed that variable x represents the local average molecular weight, provided that the number of degradation elements is sufficiently large (e.g. 140×140 in the two-dimensional (2D) model, as suggested by Gopferich [19]). For bulk-erosive polymers such as PLA, PGA and their co-polymers, since the speed of water penetration is significantly higher than the rate of hydrolysis, it is assumed that the polymer matrix is fully saturated with water in the initial state

($t = 0$) and remains immersed in an ideal solution, where the concentration of degraded products is zero at the matrix boundaries.

2.2. Matrix degradation: a stochastic hydrolysis model

In hydrolysis reaction water molecules attack the chain bonds, leading to a decrease in the average molecular weight of polymer matrix. As validated by experimental studies, polymer degradation often follows pseudo first-order kinetics [19], given by

$$M_a^t = M_a^0 e^{-\lambda t} \tag{1}$$

where M_a^0 and M_a^t are the initial ($t = 0$) and time-dependent average molecular weights, respectively. λ is defined as the degradation rate constant, which can be determined from experimental data by linear regression [31]. Therefore, one can derive the molecular weight loss function as

$$M_a^l = 1 - \frac{M_a^t}{M_a^0} = 1 - e^{-\lambda t} \tag{2}$$

where M_a^l denotes the average molecular weight loss during degradation. Following the model developed by Gopferich [19], we can consider the degradation process as a stochastic event for all the hydrolysable elements ($x_H = 1$). The average molecular weight loss described in Eq. (2) corresponds to a first order Erlang stochastic process, in which the probability density function p that defines the probability of hydrolysis of a single hydrolysable element can be calculated as

$$p(\lambda, t) = \lambda e^{-\lambda t} \tag{3}$$

However, the stochastic hydrolysis model described in Eq. (3) contains some mathematical restrictions that need to be amended for degradation modeling. Firstly, it should be noted that the first order degradation kinetics described by Eq. (1) are applicable when the polymer matrix in the initial stage has no macroscopic pores, i.e. the architectural porosity is equal to zero. Thus, for a polymer with an initial porosity α the probability density function defined in Eq. (3) is inaccurate. Since the hydrolysis probability is identical for all hydrolysable elements at any specific time t, the degradation of a porous matrix can be considered to start from a "solid" state ($\alpha = 0$) and gradually degrade to the same porosity as that of the porous matrix, as shown in Fig. 1. Therefore, the hysteretic delay t_{add} for a polymer matrix with initial porosity α can be calculated from Eq. (1) as

$$t_{add} = -\frac{\ln(M_a^t/M_a^0)}{\lambda} = \frac{\ln(1-\alpha)}{\lambda} \tag{4}$$

Secondly, to improve the computational efficiency, only hydrolysable elements ($x_H = 1$) are considered in our stochastic model. As a result, the sample space (number of hydrolysable elements) for the stochastic event described by Eq. (3) reduces as degradation evolves, leading to a probability that differs from the real event predicted in Eq. (1). For this reason, a gradual increase in the hydrolysis probability density function $p(\lambda,t)$ is used herein to accommodate the decrease in the number of hydrolysable elements. Thus, a new probability density function $P(\lambda,t)$ after considering the aforementioned difference can be defined as

$$P(\lambda, t) = \frac{\lambda e^{-\lambda(t+t_{add})}}{V(t)} = \frac{\lambda e^{-\lambda t}}{V_0 V(t)} \tag{5}$$

where $V(t)$ is the volume fraction of polymer matrix at time t and V_0 is the initial volume fraction. Consequently, both the initial architectural porosity and the porosity generated by ongoing degradation can be taken into account by increasing $P(\lambda,t)$ proportionally. For each run determining the hydrolysis state of a hydrolysable element, a random number between 0 and 1 is generated. If the random number is less than $P(\lambda,t)$, this element is considered to be hydrolyzed and its state variable x becomes 0.001 at the following time step. In contrast, if the random number is greater than $P(\lambda,t)$, this element remains unchanged and will be included in the stochastic hydrolysis process in the next step.

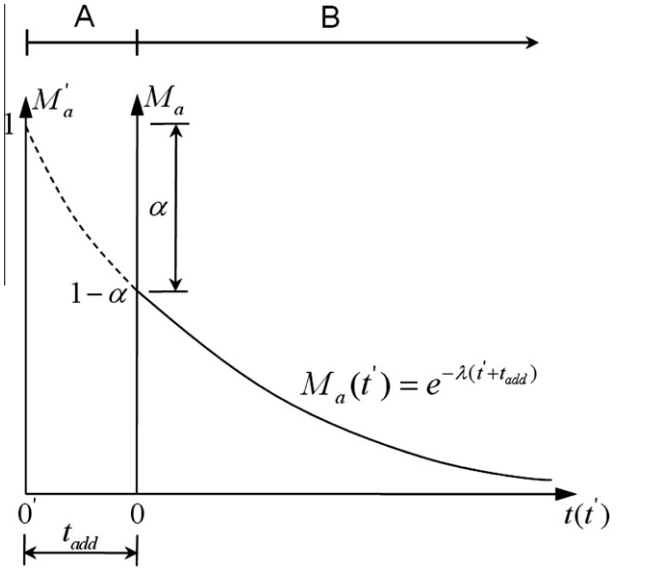

Fig. 1. A schematic diagram to determine the hysteretic delay t_{add} for a polymer matrix that has initial architectural porosity α. Since the stochastic hydrolysis model is in an elemental form and the hydrolysis probability is identical for all hydrolysable elements at any specific time t, the degradation of a porous matrix can be considered sequentially, following a process starting from the "solid" state ($\alpha = 0$) and finally reaching the same porosity as the porous one considered. Zone A: a virtual degradation process starting from a matrix without an architectural void ($\alpha = 0$). t_{add} can be calculated from Eq. (4) to correct the probability density function $p(\lambda,t)$; zone B: true simulation following the virtual stage by taking into account the hysteretic delay t_{add}.

2.3. Autocatalysis: a diffusion–reaction process

The *in vitro* tests have demonstrated that autocatalysis is of great importance in accelerating local hydrolysis, thus affecting the degradation rate of polymer devices [13]. To model the autocatalytic effect a diffusion process is established based upon the above mentioned stochastic hydrolysis model, which includes multi-fold processes, i.e. the release of hydrolyzed monomers, diffusion of the acid catalyst and acid-accelerated hydrolysis.

The time-dependent concentration of hydrolyzed monomers C_m is determined at all nodes of degradation elements and is set to zero before hydrolysis starts ($t = 0$). When chain scission takes place, monomers are released from the hydrolyzed elements. It is assumed that the polymer chains in a degradation element are completely broken down after hydrolysis, which is considered appropriate as long as the size of the degradation elements is sufficiently small [19]. Accordingly, C_m (a nodal variable) is increased by allocating the mass of degraded chains (an elemental variable $x_H - x_h$) evenly to all the adjacent nodes, provided that there is no mass loss during the hydrolysis reaction, as

$$C_{m\,new}^N = C_m^N + \frac{x_H - x_h}{n} \tag{6}$$

where C_m^N and $C_{m\,new}^N$ are the nodal values of C_m in a degraded element before and after the hydrolysis reaction, respectively. n is the number of nodes for a single degradation element.

After the monomers are released by hydrolysis, the time-dependent diffusion of these components can be predicted by Fick's second law,

$$\frac{\partial C_m}{\partial t} = \nabla(D_m \nabla C_m) + S(t) \tag{7}$$

where D_m is the diffusivity of degraded products and $S(t)$ is the source term of released monomers generated by the hydrolysis reaction. However, as a result of complex chemical reactions occurring within the polymer matrix, diffusivity should not be invariable during the degradation process. Experiments have shown that transport properties such as diffusivity are dependent on the extent of local matrix hydrolysis [24]. Herein, an exponential function is used to model such a dependency, as

$$D_m = D_m^0 e^{R_m(x_H - x)/x_H} \tag{8}$$

where D_m^0 denotes the diffusivity of degraded products prior to hydrolysis and R_m is a constant for different materials considered. As the degraded monomers are released and transported within the polymer matrix, the concentration of carboxylic functional end groups generated by monomers increases, which is considered to have a similar distribution profile to that of C_m.

Although exhaustive experimental studies have been conducted on multi-fold biodegradable polymers under different conditions, degradation rate constants that eliminate the effect of autocatalysis and size dependence of degradation have not yet been accurately measured [6]. Nevertheless, a conceptual degradation rate constant λ_0 can be defined to account for the intrinsic properties of a degradable polymer in the absence of autocatalysis and size dependence. It should be noted that, if the material and configuration remain unchanged, the matrix degradation can be considered as the following twofold process:

(1) Fundamental hydrolysis without autocatalysis, which is governed by λ_0 and can be modeled by using λ_0 in Eq. (5), instead of λ.
(2) An accelerating effect with autocatalysis, which is affected by diffusion of interior acid catalyst. According to studies by Lam et al. [13] and von Burkersroda et al. [6], autocatalysis in terms of acid catalyst concentration follows an exponential relationship based on the fundamental hydrolysis reaction.

To depict such a twofold effect another constant β is introduced to regulate the contribution of autocatalysis to match the modeling result to the known experimental data. As a result, a hybrid degradation model with both fundamental hydrolysis and an accelerating effect of autocatalysis can be formulated as

$$P_A = P_F + P_C = P_F + \beta(e^{C_m} - 1)P_F = \frac{\lambda_0 e^{-\lambda_0 t}(1 + \beta(e^{C_m - 1}))}{V_0 V(t)} \tag{9}$$

where P_A is the accelerated probability density function; P_F and P_C are the contributions due to fundamental hydrolysis and autocatalysis, respectively. As stated above, the extent of autocatalysis is governed by the diffusion process and largely depends on the device size. Unfortunately, there has as yet been no data available to identify an accurate autocatalysis-free size for commonly used biodegradable polymers. Experimental studies have shown that this critical polymer thickness might be less than 10–50 μm (depending on different diffusivities of and pathways in various polymer materials [9,32]), at which the theoretical autocatalysis-free degradation rate can be approximately achieved.

On the other hand, we adopt an empirical function to describe the exponential relationship between monomer (carboxylic acid) concentration C_m and the autocatalytic effect P_C. To better regulate the proportion between two probability density terms P_F and P_C in Eq. (9), β needs to be prescribed prior to each test and remains constant throughout the simulation. If $\beta = 0$ Eq. (9) is downgraded to Eq. (5), which implies the absence of autocatalytic effect, while as β increases the autocatalytic effect increases. Therefore, the degradation of specific polymer materials of different sizes and configurations can be modeled by choosing the appropriate values for autocatalysis-free degradation rate constant λ_0 and regulating parameter β, which will be discussed through the following illustrative examples.

3. Results and discussion

3.1. Degradation of polymer films

In this section some benchmark studies are first presented. Considering square poly(DL-lactide) films without geometrical pores ($\alpha = 0$), all boundaries are exposed to the ideal stable solution (i.e. $C_m = 0$ at matrix boundaries). Because of the double symmetry, only a quarter of the film is taken into account here. The degradation rate constant λ_0 is taken to be $8.41 \times 10^{-3}\,\mathrm{day}^{-1}$ from Pitt et al. [33] for comparison. The diffusivity D_m^0 is assumed to be $0.87 \times 10^{-7}\,\mathrm{mm^2\,s^{-1}}$ and R_m to be 8.52 for poly(DL-lactide) films, as in the literature [24,34].

In order to validate the proposed model a range of matrix sizes and parameter β were tested. Fig. 2 shows the degradation curves in terms of average molecular weight loss in these tests. Firstly, if the autocatalytic effect is not considered ($\beta = 0$), the degradation rate would be independent of the matrix size. Correspondingly, the red dashed curve shows that autocatalysis-free case has the lowest degradation rate. Secondly, for a certain value of β (e.g. $\beta = 10$ in Fig. 2a) it can be seen that the degradation rate increases substantially as the matrix size increases. Increasing β can also accelerate the degradation process, as shown in Fig. 2b.

Fig. 3 displays the mass losses in the various scenarios tested. Compared with the data shown in Fig. 2, mass loss progresses in a different way. Initially the rate of mass loss is low, followed by the accelerating mass loss due to increasing diffusivity of the hydrolyzed elements. Subsequently, the rate of mass loss decreases again, such that the curves follow the trends of corresponding average molecular weight ones. Compared with the influence of polymer size on the rate of average molecular weight loss shown in Fig. 2, it is interesting to note that the influence of size on the rate of mass loss appears somewhat different. The mass loss becomes slower as the matrix size increases, which could be mainly due to a longer diffusion path in the case of larger matrix sizes.

To better illustrate the autocatalytic effect, which can significantly influence the degradation process, internal diffusion in three more examples with different matrix sizes is presented in Fig. 4. When the matrix size is large (3 mm) the released monomers cannot rapidly diffuse out of the matrix, leading to an accumulation of carboxylic acid. Hence, a large number of pores form inside the matrix. An increase in acid catalysis near these pores can further accelerate the local hydrolysis rate, thereby generating plentiful pores of greater radii. On the other hand, when the size of polymer matrix is reduced to 200 μm, degradation proceeds differently. The degraded chains diffuse more rapidly, leading to a lower concentration of acid catalyst than that in the 3 mm case. Thus a concentration gradient of carboxylic acid from the center (lower left) to the boundaries gradually develops. Finally, a distribution with a low molecular weight core and a high molecular weight shell emerges. If the size is further decreased (e.g. 10 μm), a similar concentration gradient could appear at an early stage. As degradation progresses the matrix undergoes a nearly homogeneous hydrolytic process, with a negligible autocatalytic effect due to rapid removal of acid catalyst from the core. In this case a pure stochastic hydrolytic process is expected, as expressed in Eq. (9) with $\beta = 0$, and thus only homogeneous holes are observed. From such observations it can be noted that as the matrix size increases degradation of the polymer film switches from "homogeneous", with a nearly uniform pattern of hydrolysis, to "heterogeneous", randomly producing a number of macroscopic pores.

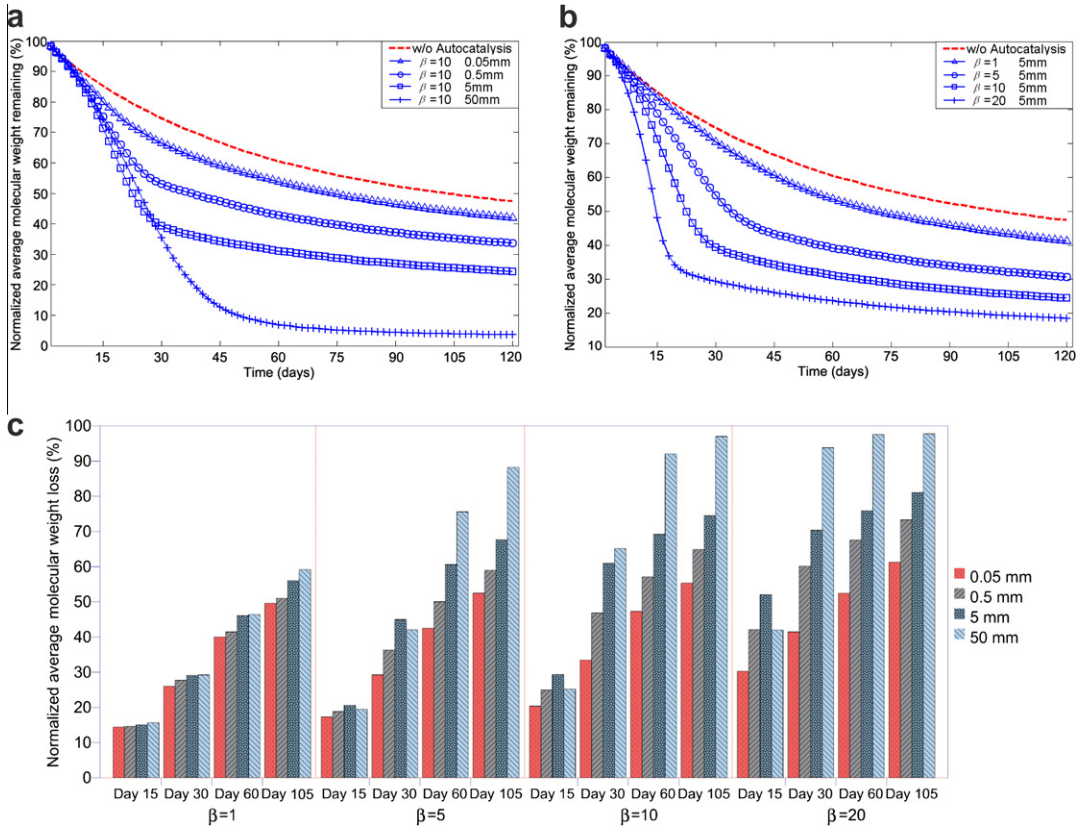

Fig. 2. Time dependence of the average molecular weight for the matrices of different sizes and having different β coefficients. (a) The effect of size on the degradation process ($\beta = 10$). (b) The role of parameter β in regulating the autocatalysis effect (5 mm). (c) The size-dependent degradation of rectangular PLA films. As β increases the degradation rate is dramatically accelerated. This could regulate the degradation process to better match the experimental data.

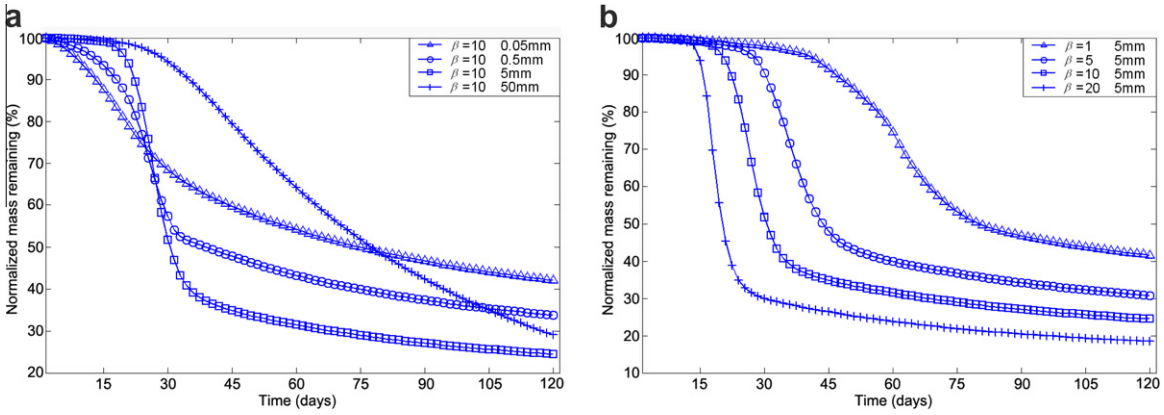

Fig. 3. The mass loss in the matrices of different sizes and with different β coefficients. (a) The effect of size on mass loss ($\beta = 10$). (b) The role of parameter β in regulating the mass loss process.

As can be seen from the results presented above, the numerical process of degradation and erosion can be regulated by choosing appropriate values for λ_0 and β. On the one hand, the autocatalysis-free rate constant λ_0 ranged from 80% to 90% of that measured experimentally, for dimensions less than the critical length, appears most appropriate in our numerical tests to match the modeling results to the experimental data. A further decrease in λ_0 could result in too great a difference between the fundamental hydrolytic process (e.g. the red dashed curve shown in Fig. 2) and experiments having a significant autocatalytic effect. On the other hand, parameter β can be used to reflect the augmentation effect resulted from autocatalysis, which further determines the correlation between the numerical and experimental results. Fig. 2c shows the influence of parameter β and the size dependence of degradation process. If β is fixed (e.g. $\beta = 5$) the polymer loses mass faster when the matrix size is increased from 0.05 to 50 mm. Furthermore, if β is increased from 1 to 20 the degradation rate accelerates dramatically. In this paper, once the autocatalysis-free rate constant λ_0 has been defined, a bisection algorithm designed to minimize the difference between the numerical results and experimental data is

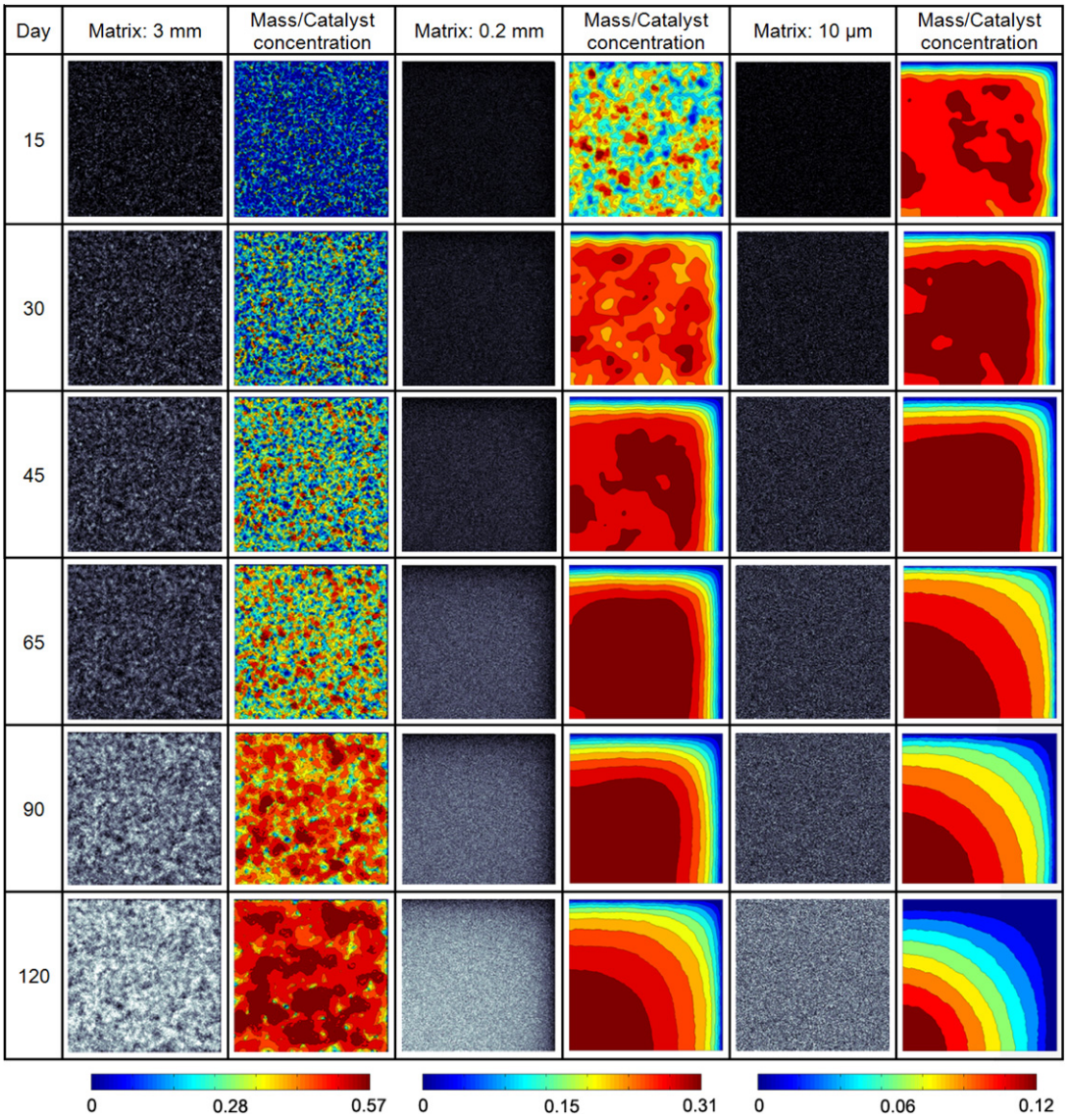

Fig. 4. Comparison of the degradation processes: matrix morphology and acid catalyst concentration ($\beta = 3$). Only a quarter of the polymer matrix is considered because of the double symmetry, in which the lower left corner of design domain is the center of the whole polymer film. Size of design domain: left, 3 mm; middle, 0.2 mm; right, 10 μm.

used to search for the optimal value of parameter β, giving a better match between numerical results and experimental data in different scenarios.

3.2. Degradation of microparticles

For controlled drug delivery systems, biodegradable polymeric microparticles can be key carriers to control the time-dependent drug and protein release rate [35,36]. In recent years there has been increasing interest in the mass transport mechanisms that may largely determine the release process. Siepmann et al. [7] characterized the polymer degradation of and drug release from drug-loaded/drug-free PLGA-based microparticles and developed a mathematical model to quantitatively describe the release process. Importantly, an autocatalytic effect was observed in both the drug-loaded/drug-free microparticles, even for those particles whose radius was less than 20 μm. Later, Klose et al. [37,38] performed systematic studies on the drug release mechanisms of porous PLGA-based microparticles and proposed that the porosity, microparticle dimensions and bulk to fluid ratio could play critical roles in regulating the degradation process. These studies revealed that the degradation rate of carrier matrix determines drug release process. However, the challenge remains how to characterize mass transport in microparticles in a quantitative way to better control and optimize drug release.

With regard to the axisymmetric condition in microparticles, only a planar problem is considered herein for the sake of simplicity. In the initial stage ($t = 0$) the state variable x for all elements inside the matrix is set as "hydrolysable" ($x_H = 1$), while the other region which represents the ambient solution is considered "void" ($x_v = 0$). The experimental parameters and data from Siepmann et al. [7] and Klose et al. [37] were chosen here for correlation purposes.

Fig. 5a shows the average molecular weight of four PLGA-based microparticles ($R_m = 7.69$ and $D_m^0 = 0.53 \times 10^{-7}$ mm^2 s^{-1} [24,34]) with different radii. The autocatalysis-free degradation rate constant λ_0 was chosen to be 0.0714 day^{-1}. After considering the acid acceleration term as given in Eq. (9), the decrease of molecular weight in four different microparticles are predicted, in which an optimal autocatalysis parameter β value of 0.92 is sought using

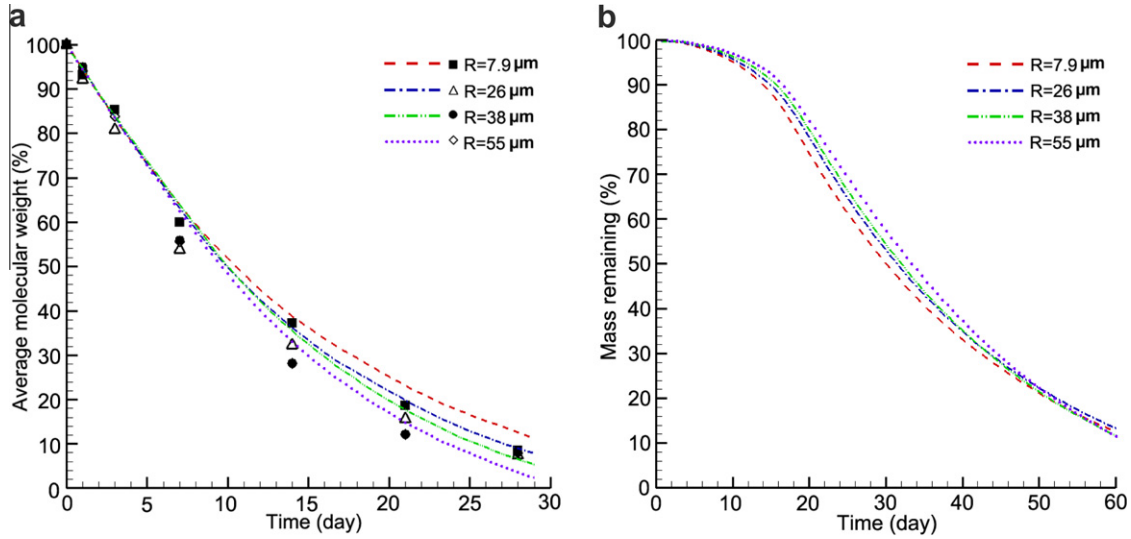

Fig. 5. Degradation of microparticles ($\lambda_0 = 0.0714$ day^{-1}, $\beta = 0.92$). The experimental results shown as scatter points are from Siepmann et al. [7]. (a) Average molecular weight of four different microparticles. As the radius increases the rate of average molecular weight loss becomes faster. (b) In contrast, in terms of mass loss from different microparticles, the rate becomes slower as the radius increases, due to the longer diffusion path.

the bisection algorithm to correlate with the experimental data. It can be seen that the numerical results in Fig. 5a show good agreement with the experimental data obtained by Siepmann et al. [7]. In the early stage ($t < 5$ days), since the same value for λ_0 is used in each test and the local concentration of carboxylic acid is low, all four tests show the similar rates of molecular weight decrease . As the degradation progresses, the larger the radius of microparticle, the faster the molecular weight loss in the matrix. A similar trend for the mass loss curves is exhibited in Fig. 5b, with a gradual increase of the loss rate, finally following the same trend as molecular weight loss.

To further investigate autocatalysis and size dependence of degradation, the mass transport profiles of smaller ($R = 7.9$ μm) and larger ($R = 55$ μm) microparticles are plotted in Fig. 6. In the early stage, although both cases have a similar overall extent of hydrolysis, the concentration patterns of degraded monomers that can form carboxyl end groups are very different. In the smaller microparticle a concentration gradient of carboxylic acid developed, with a relatively fast mass transport process due to a shorter diffusion path. In the larger microparticle, on the other hand, the degraded monomers do not immediately congregate in the core. Instead, isolated areas can be observed where higher concentration of carboxylic acid appears. As degradation progresses, more and more monomers are released. Consequently, a concentration gradient develops from the center to the solution–matrix interface in the both examples. Interestingly, it can be observed that the acid

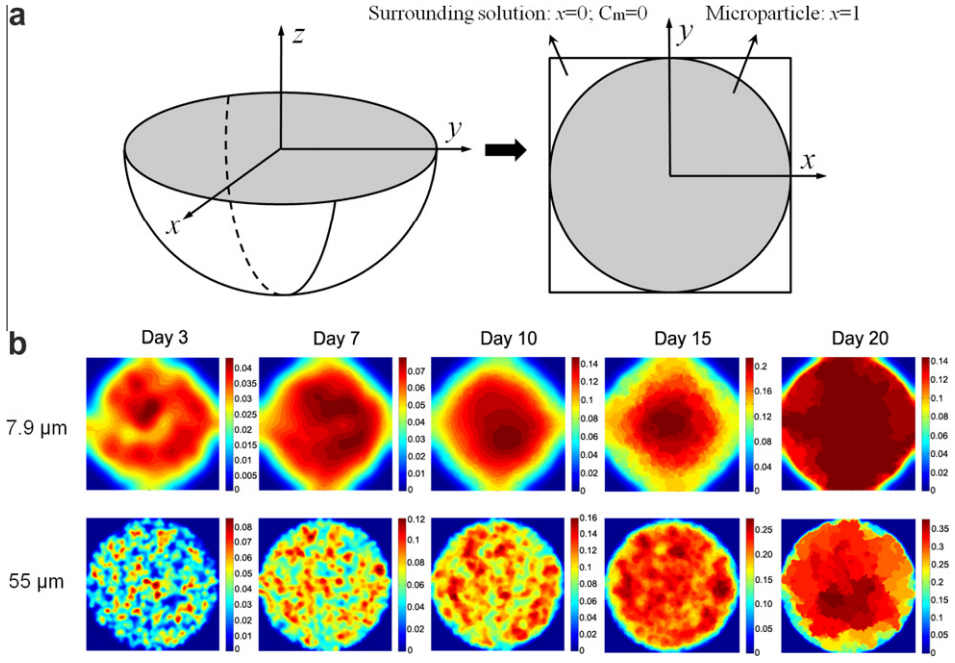

Fig. 6. Degradation of microparticles. (a) Schematic diagram for problem settings. (b) Concentration profiles of acidic monomers released from two microparticles (radii 7.9 and 55 μm) during degradation. Different scale bars are used to illustrate the concentration profiles for a better contrast.

catalyst concentration begins to descend after day 15 in the smaller microparticle, whereas the concentration of carboxylic acid continues to increase even after day 20 in the larger microparticle.

It is interesting to note that in the proposed model the concentration contours (Fig. 6) can have multiple implications as the state variable x representing elemental molecular weight is dimensionless. In fact, the degraded monomers and carboxylic acid groups that can reduce the local pH are supposed to have the same dimensionless concentration profile. Therefore, the contours of concentration gradient in Fig. 6 can also be interpreted as the pH distribution within the polymer matrix. The higher the concentration of carboxylic acid groups, the lower the pH value would be. As such, the accumulated carboxylic acid can accelerate the local hydrolysis process and, eventually, change the morphology of the microparticles in a heterogeneous fashion. Recent work in measuring micro-pH (μpH) distributions by confocal microscopy has been found particularly promising in addressing such an interesting phenomenon. Fu et al. [39] used confocal fluorescence microscopy to visualize the μpH distribution within degrading microparticles and found a diffusion controlled μpH gradient. Further, Schwendeman and co-workers [40,41] investigated the acidic μpH environment in PLGA microparticles with different lactic/glycolic acid ratios and of different sizes, in which the effect of diffusion on μpH, controlled by the microparticle size, was explored. Those works provided us with evidence that the μpH profiles due to the local concentration of released monomer are strongly related to the internal diffusion within microparticles.

3.3. Degradation of tissue engineering scaffolds

With the rapid development of micro-/nano-fabrication technologies, porous scaffolds have proven particularly promising for their superior capability of providing a desired biomimetic environment for tissue regeneration. It has been reported that microarchitectures optimized for mechanical, permeable and/or fluidic criteria can greatly improve scaffold performance, such as desired mechanical stimulation, nutrient transport and cell proliferation [42–51]. In this example the architecture of PLA scaffolds comprising a representative volume element (RVE) with a Schwarz-P surface (Fig. 7) is considered. Using the proposed model, the RVE is discretized into regular degradation elements with a three-dimensional (3D) mesh of $100 \times 100 \times 100$.

Fig. 8 plots the evolution of average molecular weights and mass losses for three different cases with RVE sizes of 50, 100 and 300 μm, respectively. It can be observed that in the early stages the degradation rate accelerates as RVE size increases. As for mass loss, larger sized matrices lose weight more slowly than smaller ones. However, as more and more degradable elements are hydrolyzed, the overall diffusion rate of larger sized matrix becomes higher and higher within the scaffold. Thus, the 300 μm scaffold loses weight faster after 100 days.

To observe the detailed degradation process the morphological changes in scaffolds with RVE of 50 μm and 300 μm are explored here. Since the scaffold architecture shown in Fig. 7 has three orthogonal symmetry planes, to illustrate mass diffusion inside the polymer material, Fig. 9 plots the morphologies of different RVEs and the corresponding concentration contours in two representative cross-sections. On day 7 the extent of hydrolysis is insignificant in both cases, thus no distinct changes can be observed in the polymer backbone except for some scattered pores. It can be seen that in the vertical section for the 50 μm case (Fig. 9a) some areas are developing a higher carboxylic acid concentration inside the solid framework of scaffold, while more, disperse areas are observed in Fig. 9b. As can be seen from the concentration contours in the horizontal sections, although some regions in the 300 μm case present an unchanged concentration pattern and almost no carboxylic acid can

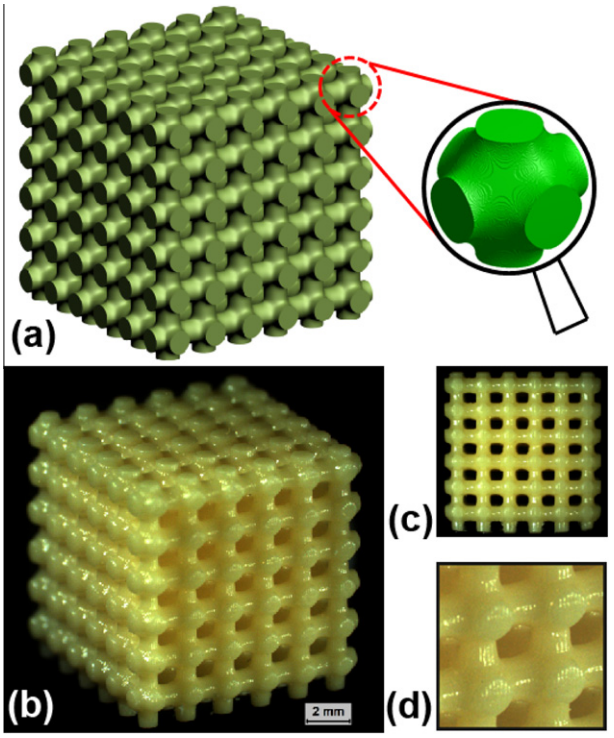

Fig. 7. 3D cellular Schwarz-P scaffold designs. (a) A cellular Schwarz-P scaffold, from macroscopic architecture to microscopic base cell. (b–d) The cellular material model constructed by solid free-form fabrication (SFF) (Perfactory® III Standard, Envisiontec, Gladbeck, Germany), using SI-300 ABS simulant material. The dimensions of base cells are scaled up in order to better reveal the architectural characteristics. This specifically designed scaffold has some exceptional characteristics in terms of optimized permeability and wall shear stress uniformity [51] which could lead to better cell adhesion and proliferation.

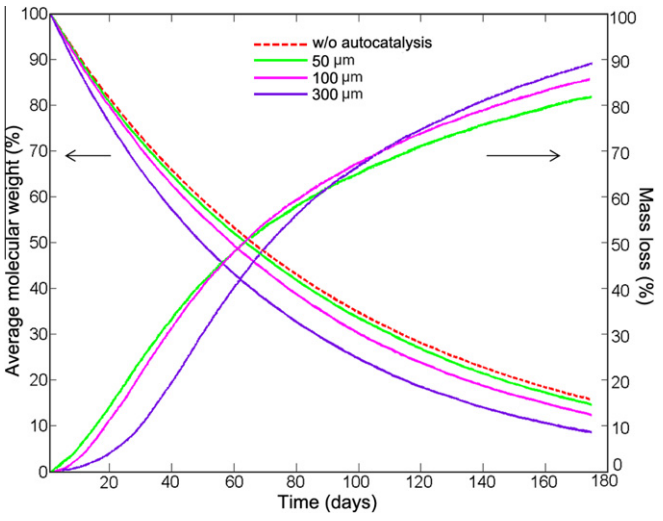

Fig. 8. The average molecular weight and mass loss curves of different Schwarz-P scaffolds (green, 50 μm; magenta, 100 μm; violet, 300 μm). The red dashed curve indicates the average molecular weight due to primary hydrolysis without an autocatalytic effect ($\lambda_0 = 0.0185\ \text{day}^{-1}$, $\beta = 2.5$).

be observed therein, many areas with a high concentration of acid catalyst appear. As degradation develops over a period of 20 days, numerous tiny pores emerge in the scaffold backbone. Meanwhile, higher levels of degraded products are generated and the carboxylic acid concentration is enhanced in the both cases. However, the concentration profiles in both sections for the 50 μm case (Fig. 9c)

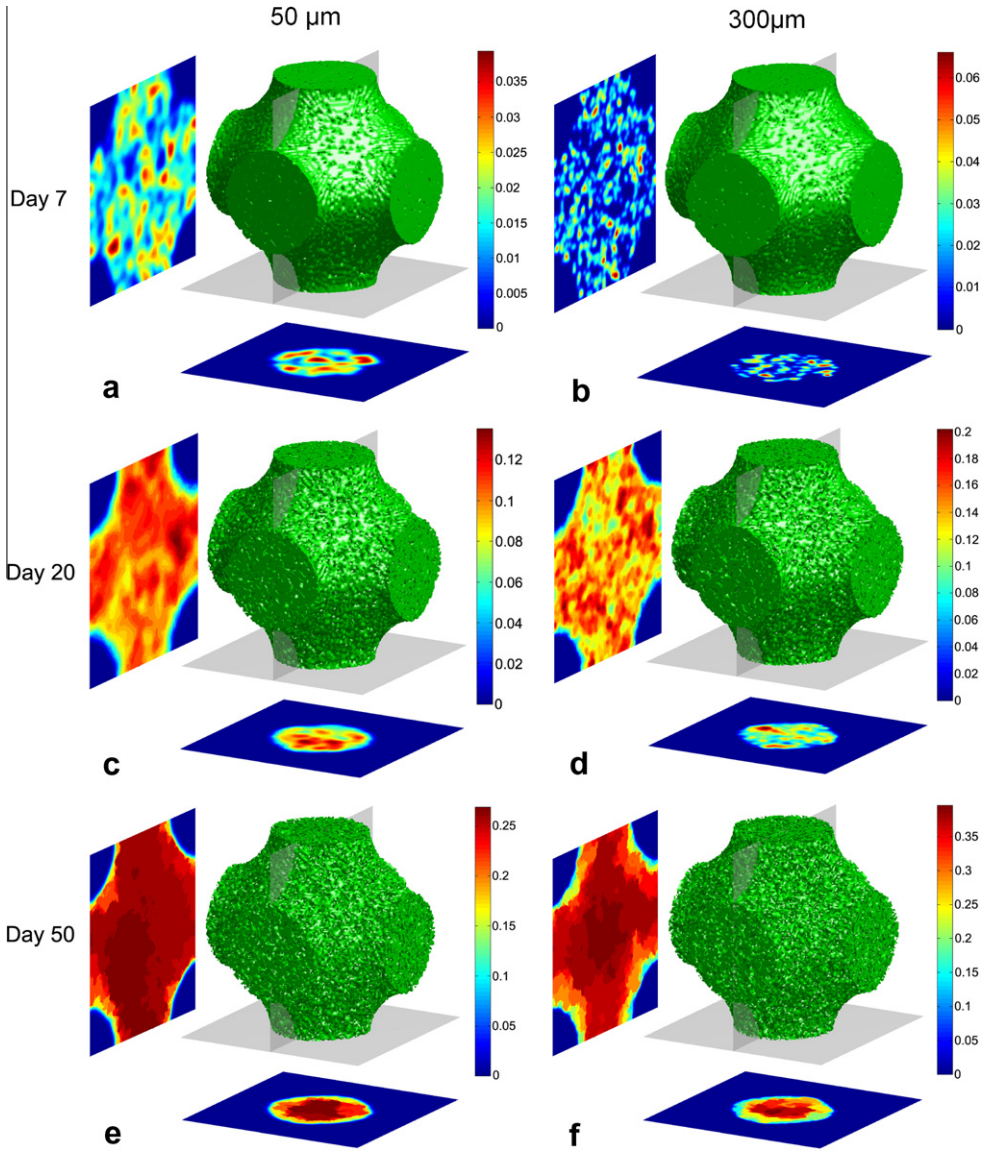

Fig. 9. The morphology and cross-sectional acidic monomer concentration of two different Schwarz-P scaffolds (architectural porosity $\alpha = 0.45$) during degradation (left, 50 μm; right, 300 μm).

appear more uniform, with a lower concentration in the peak regions than in the 300 μm case (Fig. 9d), mainly due to a shorter diffusion path. On day 50 the scaffold matrices become considerably more porous and a concentration gradient of carboxylic acid has formed from the center to matrix boundary in both cases.

The degradation processes of tissue scaffolds of different sizes shown in Figs. 8 and 9 provide us with some momentous evidence to better understand the autocatalysis and size dependence of biodegradable devices. Hydrolysis, as a fundamental reaction in polymer degradation, produces degraded monomers that can increase the concentration of carboxyl end groups. Subsequently the diffusion of hydrolysis products transports these carboxylic acid end groups within the matrix microstructures, dependent on the boundary conditions in terms of scaffold architecture and diffusion path length (size). Finally, the concentration gradient of carboxylic acid in turn accelerates the rate of hydrolysis. This suggests that, for controlled degradation systems, the fundamental hydrolysis rate and polymer architecture, as well as the matrix size, could together determine the characteristics of degradation and erosion.

4. Concluding remarks

This paper proposed a hybrid mathematical model for the degradation of biodegradable bulk-erosive devices. A stochastic hydrolysis reaction, mass transport and acid-accelerated autocatalysis were modeled together. A number of illustrative examples were presented, with potential applications for drug delivery micro-particles and tissue scaffolds. It can be concluded that the architecture and size could play a critical role in regulating the degradation rate and pathway of biodegradable devices. If the topology of a polymer matrix is complex, e.g. the surface to volume ratio is high, the acid catalyst can rapidly diffuse from the interior of the matrix, thereby reducing the degradation rate. If the size of polymer matrix is greater the acid catalyst can accumulate in the bulk, resulting in accelerated degradation therein. The concentration profiles illustrated in this paper provide important evidence to account for the mass transport characteristics in biodegradable polymers. Use of the proposed model to design a range of biodegradable devices for use as drug release systems and tissue scaffolds was illustrated.

There are several limitations to this proposed mathematical method. Certain chemical concerns, including the kinetics of hydrolysis reaction and other forms of chain scission, have not been considered. Although it has been reported that biological entities, including the delivered drug or protein [52], and mechanical loading [53] could affect polymer degradation, only natural degradation of matrix has been taken into account in this study. The status variable x and related assumptions in hydrolysis model cannot calculate the molecular weight distribution within polymer matrix. Furthermore, since the diffusive parameters used in Eq. (8) are difficult to measure experimentally and the hydrolysis model is based on average molecular weight, the size effect on mass loss might not be very accurate, although the trend agrees well with the experimental data in literature.

Acknowledgements

Support from the Australian Research Council (ARC) is greatly acknowledged. Y.C. is grateful for a Faculty Scholarship at the University of Sydney.

Appendix A. Figures with essential colour discrimination

Certain figures in this article, particularly Figs. 2–9 are difficult to interpret in black and white. The full colour images can be found in the on-line version, at doi:10.1016/j.actbio.2010.09.038.

References

[1] Hollister SJ. Porous scaffold design for tissue engineering. Nat Mater 2005;4(7):518–24.
[2] Anderson JM, Shive MS. Biodegradation and biocompatibility of PLA and PLGA microspheres. Adv Drug Delivery Rev 1997;28(1):5–24.
[3] Badylak SF, Freytes DO, Gilbert TW. Extracellular matrix as a biological scaffold material: structure and function. Acta Biomater 2009;5(1):1–13.
[4] Amass W, Amass A, Tighe B. A review of biodegradable polymers: uses, current developments in the synthesis and characterization of biodegradable polyesters, blends of biodegradable polymers and recent advances in biodegradation studies. Polym Int 1998;47(2):89–144.
[5] Tamada JA, Langer R. Erosion kinetics of hydrolytically degradable polymers. Proc Natl Acad Sci USA 1993;90(2):552–6.
[6] von Burkersroda F, Schedl L, Gopferich A. Why degradable polymers undergo surface erosion or bulk erosion. Biomaterials 2002;23(21):4221–31.
[7] Siepmann J, Elkharraz K, Siepmann F, Klose D. How autocatalysis accelerates drug release from PLGA-based microparticles: a quantitative treatment. Biomacromolecules 2005;6(4):2312–9.
[8] Lee M, Wu BM, Dunn JCY. Effect of scaffold architecture and pore size on smooth muscle cell growth. J Biomed Mater Res Part A 2008;87A(4):1010–6.
[9] Grizzi I, Garreau H, Li S, Vert M. Hydrolytic degradation of devices based on poly(DL-lactic acid) size dependence. Biomaterials 1995;16(4):305–11.
[10] Witt C, Kissel T. Morphological characterization of microspheres, films and implants prepared from poly(lactide-co-glycolide) and ABA triblock copolymers: is the erosion controlled by degradation, swelling or diffusion? Eur J Pharm Biopharm 2001;51(3):171–81.
[11] Olivares AL, Marshal E, Planell JA, Lacroix D. Finite element study of scaffold architecture design and culture conditions for tissue engineering. Biomaterials 2009;30(30):6142–9.
[12] Chen X, Ooi CP. Hydrolytic degradation and drug release properties of ganciclovir-loaded biodegradable microspheres. Acta Biomater 2008;4(4):1046–56.
[13] Lam CXF, Savalani MM, Teoh SH, Hutmacher DW. Dynamics of in vitro polymer degradation of polycaprolactone-based scaffolds: accelerated versus simulated physiological conditions. Biomed Mater 2008;3(3).
[14] Agrawal CM, McKinney JS, Lanctot D, Athanasiou KA. Effects of fluid flow on the in vitro degradation kinetics of biodegradable scaffolds for tissue engineering. Biomaterials 2000;21(23):2443–52.
[15] Siepmann J, Gopferich A. Mathematical modeling of bioerodible, polymeric drug delivery systems. Adv Drug Delivery Rev 2001;48(2–3):229–47.
[16] Zygourakis K. Development and temporal evolution of erosion fronts in bioerodible controlled release devices. Chem Eng Sci 1990;45(8):2359–66.
[17] Zygourakis K, Markenscoff PA. Computer-aided design of bioerodible devices with optimal release characteristics: a cellular automata approach. Biomaterials 1996;17(2):125–35.
[18] Gopferich A, Langer R. Modeling of polymer erosion. Macromolecules 1993;26(16):4105–12.
[19] Gopferich A. Polymer bulk erosion. Macromolecules 1997;30(9):2598–604.
[20] Gopferich A. Mechanisms of polymer degradation and erosion. Biomaterials 1996;17(2):103–14.
[21] Bertrand N, Leclair G, Hildgen P. Modeling drug release from bioerodible microspheres using a cellular automation. Int J Pharm 2007;343(1–2):196–207.
[22] Barat A, Crane M, Ruskin HJ. Quantitative multi-agent models for simulating protein release from PLGA bioerodible nano- and microspheres. J Pharm Biomed Anal 2008;48(2):361–8.
[23] Arifin DY, Lee LY, Wang CH. Mathematical modeling and simulation of drug release from microspheres: implications to drug delivery systems. Adv Drug Delivery Rev 2006;58(12–13):1274–325.
[24] Thombre AG, Himmelstein KJ. A simultaneous transport–reaction model for controlled drug delivery from catalyzed bioerodible polymer matrices. AICHE J 1985;31(5):759–66.
[25] Wang Y, Pan JZ, Han XX, Sinka C, Ding LF. A phenomenological model for the degradation of biodegradable polymers. Biomaterials 2008;29(23):3393–401.
[26] Han XX, Pan JZ. A model for simultaneous crystallisation and biodegradation of biodegradable polymers. Biomaterials 2009;30(3):423–30.
[27] Rothstein SN, Federspiel WJ, Little SR. A unified mathematical model for the prediction of controlled release from surface and bulk eroding polymer matrices. Biomaterials 2009;30(8):1657–64.
[28] Soares JS, Zunino P. A mixture model for water uptake, degradation, erosion and drug release from polydisperse polymeric networks. Biomaterials 2010;31(11):3032–42.
[29] Hutmacher DW, Sittinger M, Risbud MV. Scaffold-based tissue engineering: rationale for computer-aided design and solid free-form fabrication systems. Trends Biotechnol 2004;22(7):354–62.
[30] Sun W, Darling A, Starly B, Nam J. Computer-aided tissue engineering: overview, scope and challenges. Biotechnol Appl Biochem 2004;39:29–47.
[31] Tracy MA, Ward KL, Firouzabadian L, Wang Y, Dong N, Qian R, et al. Factors affecting the degradation rate of poly(lactide-co-glycolide) microspheres in vivo and in vitro. Biomaterials 1999;20(11):1057–62.
[32] Jonnalagadda S, Robinson DH. Effect of thickness and PEG addition on the hydrolytic degradation of PLLA. J Biomater Sci Polym Ed 2004;15(10):1317–26.
[33] Pitt CG, Gratzl MM, Kimmel GL, Surles J, Schindler A. Aliphatic polyesters II. The degradation of poly(DL-lactide), poly(epsilon-caprolactone), and their copolymers in vivo. Biomaterials 1981;2(4):215–20.
[34] Neogi P. Diffusion in polymers. New York: Marcel Dekker; 1996.
[35] Kumar M. Nano and microparticles as controlled drug delivery devices. J Pharm Pharm Sci 2000;3(2):234–58.
[36] Sinha VR, Trehan A. Biodegradable microspheres for protein delivery. J Controlled Release 2003;90(3):261–80.
[37] Klose D, Siepmann F, Elkharraz K, Krenzlin S, Siepmann J. How porosity and size affect the drug release mechanisms from PLIGA-based microparticles. Int J Pharm 2006;314(2):198–206.
[38] Klose D, Siepmann F, Willart JF, Descamps M, Siepmann J. Drug release from PLGA-based microparticles: effects of the "microparticle:bulk fluid" ratio. Int J Pharm 2010;383(1–2):123–31.
[39] Fu K, Pack DW, Klibanov AM, Langer R. Visual evidence of acidic environment within degrading poly(lactic-co-glycolic acid) (PLGA) microspheres. Pharm Res 2000;17(1):100–6.
[40] Li L, Schwendeman SP. Mapping neutral microclimate pH in PLGA microspheres. J Controlled Release 2005;101(1–3):163–73.
[41] Ding AG, Schwendeman SP. Acidic microclimate pH distribution in PLGA microspheres monitored by confocal laser scanning microscopy. Pharm Res 2008;25(9):2041–52.
[42] Hollister SJ, Maddox RD, Taboas JM. Optimal design and fabrication of scaffolds to mimic tissue properties and satisfy biological constraints. Biomaterials 2002;23(20):4095–103.
[43] Adachi T, Osako Y, Tanaka M, Hojo M, Hollister SJ. Framework for optimal design of porous scaffold microstructure by computational simulation of bone regeneration. Biomaterials 2006;27(21):3964–72.
[44] Hollister SJ. Scaffold design and manufacturing: from concept to clinic. Adv Mater 2009;21(32–33):3330–42.
[45] Karageorgiou V, Kaplan D. Porosity of 3D biomaterial scaffolds and osteogenesis. Biomaterials 2005;26(27):5474–91.
[46] Sturm S, Zhou SW, Mai YW, Li Q. On stiffness of scaffolds for bone tissue engineering – a numerical study. J Biomech 2010;43:1738–44.
[47] Lacroix D, Planell JA, Prendergast PJ. Computer-aided design and finite-element modelling of biomaterial scaffolds for bone tissue engineering. Philos Trans R Soc A Math Phys Eng Sci 2009;367(1895):1993–2009.
[48] Hutmacher DW, Schantz JT, Lam CXF, Tan KC, Lim TC. State of the art and future directions of scaffold-based bone engineering from a biomaterials perspective. J Tissue Eng Regen Med 2007;1(4):245–60.
[49] Sanz-Herrera JA, Garcia-Aznar JM, Doblare M. On scaffold designing for bone regeneration: a computational multiscale approach. Acta Biomater 2009;5(1):219–29.
[50] McIntosh L, Cordell JM, Johnson AJW. Impact of bone geometry on effective properties of bone scaffolds. Acta Biomater 2009;5(2):680–92.
[51] Chen YH, Zhou SW, Cadman J, Li Q. Design of cellular porous biomaterials for wall shear stress criterion. Biotechnol Bioeng 2010;107(4):737–46.
[52] Uhrich KE, Cannizzaro SM, Langer RS, Shakesheff KM. Polymeric systems for controlled drug release. Chem Rev 1999;99(11):3181–98.
[53] Fan YB, Li P, Zeng L, Huang XJ. Effects of mechanical load on the degradation of poly(D,L-lactic acid) foam. Polym Degrad Stabil 2008;93(3):677–83.